

pubs.acs.org/Macromolecules Article

# Structurally Asymmetric Porous Carbon Materials with Ordered Top Surface Layers from Nonequilibrium Block Copolymer Self-Assembly

Sarah A. Hesse, Peter A. Beaucage, Detlef-M. Smilgies, and Ulrich Wiesner\*



Cite This: Macromolecules 2021, 54, 2979-2991



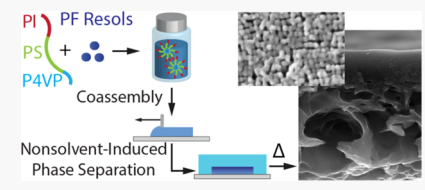
**ACCESS** 

Metrics & More



Supporting Information

**ABSTRACT:** Inorganic materials with asymmetric pore structures provide increased accessibility and flux, making them attractive for applications in energy conversion and storage, separations, and catalysis. Non-equilibrium-based block copolymer structure-directed self-assembly approaches provide routes to obtaining such materials. We report a one-pot synthesis using the co-assembly and non-solvent-induced phase separation (CNIPS) of poly(isoprene)-b-poly(styrene)-b-poly(4-vinylpyridine) (ISV) triblock terpolymer and phenol formaldehyde resols. After heat-treatment, carbon materials with



asymmetric pore structures result. They have a mesoporous top surface atop a porous support with graded porosity along the film normal. The walls of the macroporous support are also mesoporous, providing an additional structural hierarchy and increased specific surface area. We demonstrate how successfully navigating the pathway complexity associated with the nonequilibrium approach of CNIPS enables switching from disordered to ordered top surfaces in the as-made organic—organic hybrids and resulting carbon materials after thermal treatments. To that end, a combination of ex situ transmission small-angle X-ray scattering (SAXS) of the membrane dope solutions, in situ grazing-incidence SAXS (GISAXS) after dope solution blading and during solvent evaporation, and scanning electron microscopy (SEM) of the final membrane structures was used. We expect the final porous carbon materials exhibiting a combination of asymmetric, hierarchical pore structures and well-defined mesoporosity throughout the material to be of interest for a number of applications, including batteries, fuel cells, electrochemical double-layer capacitors, and as catalyst supports.

#### INTRODUCTION

Porous inorganic materials have gained attention in applications ranging from energy conversion and storage to catalysis to separations. 1,2 Porous carbon materials, a class of inorganic materials, find use in a broad range of applications including batteries, fuel cells, electrochemical double-layer capacitors (EDLCs), and gas separation due to their favorable chemical and physical properties such as high chemical resistance, compatibility with polymers, easy processability, and electrical and thermal conductivity.<sup>3-6</sup> Initial studies used a silica template as a mold to make ordered mesoporous carbon materials.<sup>7,8</sup> These initial hard-templating routes involve multiple processing steps, however, including the oftentimes highly chemically hazardous removal of the template. For this reason, various soft-templating approaches have been developed to fabricate ordered mesoporous carbons. These studies often utilize the self-assembly (SA) of block copolymers (BCPs) as structure-directing agents for organic carbon precursors, such as phenol formaldehyde resols or resorcinol resols. 10-13

A number of studies have focused on creating hierarchical materials, often with a combination of macro-, meso-, and microporosity, in order to maximize surface area. However, accessibility and pore utilization in such hierarchical systems remain an issue for applications ranging from separations to energy storage. For example, simultaneously meso- and microporous carbon is a hierarchical material with high surface area and resulting high energy density when used to make

EDLCs. Yet the material can only realize these improved energy densities at low scan rates due to limited pore accessibility at fast rates. 15

This issue of increased accessibility/flux in high-surface-area porous materials can be addressed by engineering structurally asymmetric porous structures. One approach which can be used to obtain such structurally asymmetric materials is an industrially widely used and scalable approach called nonsolvent-induced phase separation (NIPS). Traditionally, NIPS has only been used with homopolymers such as polyacrylonitrile (PAN), which, upon heat-treatment, can yield carbon structures with an asymmetric porosity profile. 16-19 These structurally asymmetric carbon materials consist of macro- to micropores and are thus hierarchical. However, because these structures lack well-defined mesopores everywhere, they face pore accessibility restrictions. 17,19 Further, the traditional NIPS process does not provide for an obvious approach to structuredirecting other nonpolymeric materials (e.g., sol-gel-derived inorganic nanoparticles), and thus, obtaining a wide library of

Received: December 9, 2020 Revised: February 14, 2021 Published: March 4, 2021



structurally asymmetric inorganic structures remains challenging.

An alternative approach pursued in this study combines the NIPS process with BCP SA in a process called self-assembly and non-solvent-induced phase separation (SNIPS) - a nonequilibrium process pioneered in 2007 by Peinemann et al. using a poly(styrene)-b-poly(2-vinylpyridine) diblock copolymer (SV) system. <sup>20,21</sup> The approach was subsequently extended to ABC triblock terpolymer poly(isoprene)-b-poly-(styrene)-b-poly(4-vinylpyridine) (PI-b-PS-b-P4VP) in order to improve membrane mechanical properties. 22,23 The SNIPS process was originally employed for the generation of ultrafiltration (UF) membranes and combines the industrially well-utilized and scalable NIPS process with BCP SA resulting in high-flux and high-resolution UF membranes. 20,22,23 To that end, BCPs are dissolved in a selective solvent mixture. The resulting micellar solution is then blade-cast/doctor bladed and allowed to evaporate for a short period of time, which introduces a polymer concentration gradient along the film normal. The films are then precipitated in a nonsolvent bath, typically water, thereby forming a porous structural gradient frozen into a polymer glass. When the formation parameters are tuned appropriately, the resulting membranes possess wellordered top surfaces with narrow pore size distribution, which continuously evolve into a substructure with increasing pore size along the film normal from meso- to macropores. Gu et al. used such BCP membranes as templates to deposit metals like nickel or copper, or carbon precursors, generating the first asymmetric porous inorganic membrane materials with a structural hierarchy after additional thermal processing.<sup>2</sup>

In order to decrease the number of processing steps in asymmetric porous organic—inorganic hybrid material formation, a process first reported by Gu *et al.* called CNIPS—co-assembly and non-solvent-induced phase separation—was developed. This process is similar to the SNIPS process. However, instead of using just BCPs in the casting solutions, BCPs are employed as structure-directing agents together with organic or inorganic precursor materials in the casting solutions, thereby eliminating time-consuming post-membrane formation processing steps. This early work by Gu *et al.* only looked at the hybrid membranes but did not demonstrate conversions into purely inorganic membranes.

In 2015, Hesse *et al.* used the CNIPS process to create asymmetric porous carbon materials with a hierarchy of structure.<sup>26</sup> PI-*b*-PS-*b*-P4VP (ISV) triblock terpolymer and phenol formaldehyde resols carbon precursors (resols) were combined in a one-pot solution, subjected to the CNIPS process and subsequently heat-treated to both cross-link the phenol formaldehyde resols and remove the polymer. The expectation was to obtain carbon materials with an ordered top surface as is characteristic of materials made *via* the combination of BCP SA and NIPS. Unfortunately, while this proof-of-principle study yielded the characteristic asymmetric pore structure, no formation conditions were found to obtain membranes with periodically ordered pores in the top surface layer of the resulting carbon materials.

It is the periodic pore order in the top-separation layer together with narrow pore size distributions, however, that sets SNIPS/CNIPS membranes apart from conventional UF membranes. This combination leads to maximum pore density, in turn providing high flux, which together with high resolution from narrow pore size distributions enables advanced membrane performance.<sup>27</sup> The high pore density leading to

high surface area and flux and the asymmetric pore structure leading to enhanced transport and surface accessibility are two factors that also need to be balanced for optimal performance in electrochemical energy storage (EES) devices.

The current study describes in-depth investigations into the early formation stages of CNIPS-derived structurally asymmetric porous carbon materials from an ISV + resols system in order to generate a deeper understanding of the processes and parameters controlling periodic pore order in the top surfaces of these asymmetric membranes. Hesse et al. have recently demonstrated that these CNIPS-derived materials show promise for obtaining both high surface area and fast transport.<sup>28</sup> Titanium nitride (TiN) and carbon materials were created that are highly conductive (TiN, carbon), and in some materials, superconducting (TiN). These materials combined an asymmetric, hierarchical pore structure with well-defined mesoporosity throughout the material. When used as an EDLC, the fast transport through TiN provided high capacity retention at high scan rates leading to state-of-the-art power density (28.2 kW kg<sup>-1</sup>) at competitive energy density (7.3 W-h kg<sup>-1</sup>). For asymmetric carbon membranes, a recordsetting power density (287.9 kW kg<sup>-1</sup>) at 14.5 W-h kg<sup>-1</sup> was achieved. These results demonstrated the significant advantages of such asymmetric pore structures for energy conversion and storage as they address the tradeoff between high surface area and high pore accessibility.

In the current study, we take a step back and demonstrate that the fundamental understanding of the early formation stages enables the generation of as-made hybrid materials as well as asymmetric carbon membranes with highly ordered top surface pores. We anticipate that these results will help to transfer the benefits of scalable SNIPS/CNIPS type membrane formation processes into a host of other porous inorganic materials with structural pore asymmetry combined with mesopores throughout, thereby opening up pathways for new applications (e.g., in separations and energy storage and conversion) not accessible for purely polymer-organic membrane materials.

## EXPERIMENTAL SECTION

Materials Synthesis/Preparation. Materials. Materials were used as received except as otherwise indicated. Anhydrous (99.9%) grades of tetrahydrofuran (THF) and 1,4-dioxane (DOX) were purchased from Sigma-Aldrich. Deionized (DI) water with a resistivity of 18.2 MΩ cm was used as the nonsolvent precipitation bath. The following chemicals were used for the synthesis of phenol formaldehyde resols: phenol (Sigma-Aldrich, purified by redistillation, ≥99%), formalin solution (Sigma-Aldrich, ACS reagent, 37 wt % in water, containing 10-15% methanol as a stabilizer to prevent polymerization), sodium hydroxide (Sigma-Aldrich, reagent grade, ≥98% pellets anhydrous), and para-toluene sulfonic acid monohydrate (Sigma-Aldrich, ACS reagent, ≥98.5%).

Polymer Synthesis and Characterization. The PI-*b*-PS-*b*-P4VP (ISV) triblock terpolymer used in this study was synthesized *via* sequential living anionic polymerization as previously reported. The polymer had a molar mass of 95 kg mol<sup>-1</sup> with 29 vol % PI, 57 vol % PS, 14 vol % P4VP, and a polydispersity index (PDI) of 1.2. A Varian INOVA 400 MHz <sup>1</sup>H solution nuclear magnetic resonance (<sup>1</sup>H NMR) spectrometer was used to determine the block fractions of each block using chloroform-*d* as solvent (D, 99.8%, Cambridge Isotope Laboratories). A Waters ambient-temperature gel permeation chromatograph (GPC) equipped with a Waters 410 differential refractive index (RI) detector (flow rate 1 mL min<sup>-1</sup>) was used to analyze the ISV polydispersity using polystyrene standards for PDI determination. THF was used as the solvent. Overall ISV molar mass

was obtained using the molar mass of the PI block (determined with GPC using PI standards) combined with the NMR results of the molar ratios of the different blocks.

Solution Preparation. ISV solutions were prepared by dissolving ISV at various concentrations in a solvent mixture of DOX/THF (7:3 by mass, referred to herein by weight or by wt) and stirred to obtain homogeneous solutions. Oligomeric phenol-formaldehyde resols with a molar mass of less than 500 g mol<sup>-1</sup> were synthesized using a procedure described elsewhere. <sup>13,26,28–30</sup> A stock solution of 25 wt % resols in DOX and a stock solution of 25 wt % resols in THF were prepared and combined in a 7:3 weight ratio to obtain a 25 wt % resols solution in DOX/THF (7:3 by weight). In the so-called "simultaneous method", appropriate amounts of ISV powder and resols stock solution were combined to achieve the desired ISV/resols ratios (typically 2:1 by weight; see text for details), and DOX/THF (7:3 by weight) was immediately added before dissolution of all the ISV was achieved to reach the desired polymer concentrations. In the so-called "consecutive method", ISV was first dissolved in DOX/THF (7:3 by weight) to obtain a homogeneous solution, to which the resols stock solution was added thereafter to obtain the targeted ISV/ resols weight ratio (typically 2:1). All solution concentrations used for ISV + resols refer to the ISV plus resols overall weight ratio in 7:3 DOX/THF.

Membrane Casting. Self-assembly/co-assembly and non-solventinduced phase separation (S/CNIPS) was used to prepare the membranes. As described in the Results and Discussion section, two substrate temperatures (room temperature (RT) or 30 °C) and humidity environments (<28% or ≈70%) were used. However, the general process remained the same. The casting solution was pipetted onto a glass substrate (75 × 51 mm), a film was cast with a doctor blade (by hand) using a gate height (height between the substrate and casting blade) between 200 and 230  $\mu$ m. The membranes typically covered about 20 × 20 mm of the substrate. The blading process typically took a few seconds, i.e., substantially shorter than the evaporation times. After various evaporation times (see main text), the films were plunged (by hand) into a nonsolvent DI water bath to allow for precipitation (usually for 30 s). In the case of overnight stirring (e.g., see Figure 4), membranes were stirred in DI water overnight allowing for the dissolution of resols out of the membranes, effectively resulting in ISV membranes (with negligible amounts of resols). Please note that the resulting DI water bath contains trace DOX, a persistent organic pollutant, and should be disposed appropriately.

**Temperature Processing.** The membranes were dried and heated in a convection oven to cross-link the resols at a temperature of 130 °C for about 24 h. This step was followed by a heat-treatment step in a flow furnace using nitrogen as the flow gas. The temperature profile for this carbonizing step was 1 °C min<sup>-1</sup> to 600 °C. The temperature was held at 600 °C for 3 h before being further ramped at 5 °C min<sup>-1</sup> to 900 °C. The furnace was then kept at 900 °C for 3 h before being allowed to cool back to room temperature at an ambient rate.

# **■ MATERIALS CHARACTERIZATION**

Small-Angle X-ray Scattering (SAXS) of Solutions. Transmission SAXS measurements were performed at the G1 station of the Cornell High Energy Synchrotron Source (CHESS) with a typical beam energy of 9.8 keV and a sample-to-detector distance of about 2 m. The precise sample—detector distance was determined for each configuration using silver behenate as a standard. Samples were loaded in 0.9 mm glass capillaries (Charles Supper Co.), flame-sealed, and sealed with epoxy as a secondary seal. Two-dimensional scattering patterns were collected on either a Dectris Pilatus 3300K or a Dectris Eiger 1M pixel array detector. Patterns were azimuthally integrated and plotted using the Nika and Irena software packages for Igor Pro.  $^{31,32}$  The scattering vector q is defined as  $q = (4\pi/\lambda)\sin\theta$ , where  $\theta$  is half of the scattering angle. Reported lattice parameters were determined by fitting the primary peak with a Gaussian function and converting the position to a lattice parameter assuming the indicated

lattice. For the body-centered cubic (BCC) lattice, the lattice parameter, a, was determined using  $a = (2\pi/q^*)\cdot\sqrt{(2)}$  assuming that the primary observed peak is the (110).

In Situ Grazing-Incidence Small-Angle X-ray Scattering (GISAXS). In situ GISAXS experiments were performed at the DI station of CHESS using a custom-built doctor blade setup as detailed by Smilgies et al.<sup>33</sup> A schematic of the experimental setup is provided elsewhere.34 Solutions were cast by an automated doctor blade spreading the polymer solution across a glass substrate at 7500  $\mu m$ s<sup>-1</sup>. Gate heights (coating gap between the substrate and the blade) of 203 or 229 µm were used. In situ GISAXS data were collected almost immediately after casting using a Pilatus 200K detector and exposure times of 1 s at 3 or 5 s intervals, between which the shutter was closed to limit radiation exposure of the sample. Representative selected intervals are shown in the figures. Incident angles of 0.12 to 0.15° were used, slightly below the critical angle of the glass substrate. GISAXS patterns are plotted against the scattering vector magnitude, q, with  $q = 4\pi \sin\theta/\lambda$ , where  $\theta$  is half of the total scattering angle and  $\lambda$  is the X-ray wavelength (1.16 or 1.17 Å). The software that was used to both plot the data and index the patterns to determine the lattice parameter is called indexGIXS.<sup>35,36</sup> In order to obtain the lattice parameters, a, of cubic lattices from the positions of the primary peak, q\*, the following equations were employed: simple cubic (SC) lattice:  $a = 2\pi/q^*$  (assuming the primary peak is the (100)); for a BCC lattice:  $a = (2\pi/q^*) \cdot \sqrt{(2)}$  (assuming the primary peak is the (111)).

SEM Analysis. Scanning electron microscopy (SEM) micrographs were obtained using either a TESCAN MIRA3 FE-SEM using an inlens detector and an accelerating voltage of 5–15 kV or a ZEISS Gemini 500 scanning electron microscope and a voltage of 2 kV. The as-made and post-130 °C-treated samples were coated with gold—palladium prior to imaging. SEM images were brightness/contrast-adjusted. Pore-to-pore distances were calculated by fast Fourier transform (FFT) analysis of the SEM micrographs (using the raw data, *i.e.*, without post-SEM brightness/contrast adjustment) followed by radial integration using ImageJ with the Radial Profile plugin (Philippe Carl).

Thermogravimetric Analysis. Analysis was conducted on a TA Instruments Q500 thermogravimetric analyzer (TGA) under nitrogen flow. The temperature was ramped from room temperature at 1 °C min<sup>-1</sup> to 600 °C, holding isothermally at 600 °C for 3 h and then further ramping up at 5 °C min<sup>-1</sup> to 900 °C. The furnace was then held at 900 °C for 3 h before being allowed to cool back to room temperature at an ambient rate.

**Nitrogen Sorption.** Nitrogen adsorption—desorption isotherms of the porous carbon materials were recorded using a Micromeritics ASAP 2020 surface area and porosity analyzer at -196 °C. The specific surface areas were determined following the Brunauer—Emmett—Teller (BET) method. <sup>37,38</sup> Barrett—Joyner—Halenda (BJH) analysis was used to determine the pore size distributions. <sup>39</sup> The reported errors result from the standard deviation from weighing each material several times. The standard deviation of the full width at halfmax (fwhm) is a result of fitting the pore size distribution with a least-squares fit to a Gaussian function in Igor Pro.

# ■ RESULTS AND DISCUSSION

Graded meso- to macroporous carbon materials with structural asymmetry, referred to in the following as CGM-Cs (carbon-based Cornell Graded Materials), <sup>24,26</sup> were obtained from a non-equilibrium-type process using the combination of co-assembly and non-solvent-induced phase separation (CNIPS) of triblock terpolymer poly(isoprene)-block-poly(styrene)-block-poly(4-vinylpyridine) (ISV) with phenol formaldehyde resols and a subsequent series of heat-treatments (Figure 1). The triblock terpolymer ISV employed here was synthesized via previously reported sequential anionic polymerization.<sup>23</sup> The polymer had a molar mass of 95 kg mol<sup>-1</sup> with 29 vol % poly(isoprene) (PI), 57 vol % poly(styrene) (PS), and 14 vol

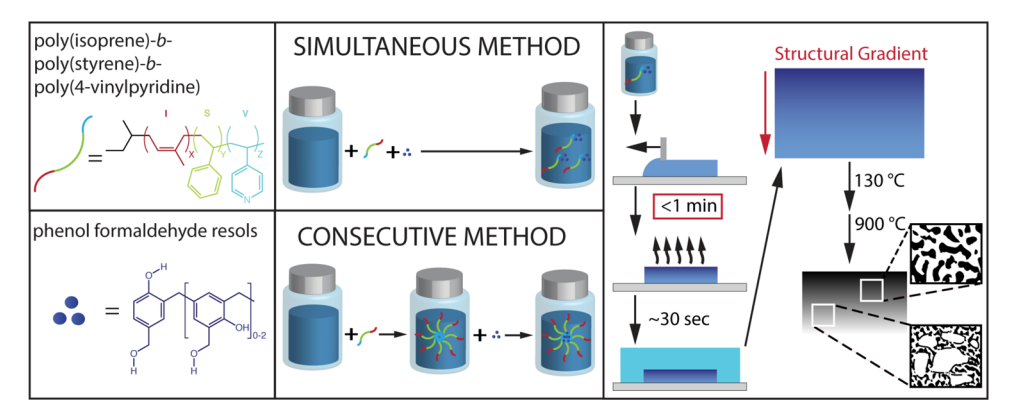


**Figure 1.** Schematic representation of chemical components and CNIPS process pathways. Typically, a 2:1 weight ratio of ISV/resols in a 7:3 ratio (by weight) of DOX/THF was cast onto a glass slide. The starting solutions were prepared by either a "simultaneous" or a "consecutive method" as indicated. The solutions were evaporated for a specific amount of time to induce a concentration gradient and plunged into a DI water bath whereby the polymer was precipitated, converting the concentration gradient into a structural gradient. The resulting asymmetric membranes were subjected to a series of heat-treatments to cross-link the resols (130 °C) and carbonize the system (900 °C). The BCP decomposes during carbonization leading to shrinkage and additional mesoporosity on the way to final CGM-Cs.

% poly(4-vinylpyridine) (P4VP) and a polydispersity index (PDI) of 1.2. Resols with a molar mass of less than 500 g mol<sup>-1</sup> were synthesized as described previously and used as thermally cross-linkable carbon precursor materials. <sup>13,26</sup>

The CNIPS process and heat-treatment (Figure 1) for preparing CGM-C materials followed previously reported protocols.<sup>26</sup> Typically, a 2:1 ratio by weight of ISV/resols in a 7:3 ratio by weight of DOX/THF was prepared into coassembled solutions. After stirring, the homogeneous solutions were cast onto glass slides using a doctor blade and allowed to evaporate for a specific amount of time. This introduced a concentration gradient along the film-normal direction. Hereafter, the films were plunged into a nonsolvent, i.e., a deionized (DI) water bath. The membranes were only immersed in water for short periods of time ( $\approx$ 30 s) to avoid dissolution of the hydrophilic resols in water. This concluded the CNIPS part of the process. The ISV + resols hybrid membranes were then subjected to a series of heattreatments as described in the Experimental Section. They were first dried and cured at 130 °C to induce cross-linking of the resols. Cross-linking is essential to provide a stable structure for the subsequent carbonization step, which was achieved by heating materials up to 900 °C.

Two different methods were employed for making the casting solutions (Figure 1, middle). In the "simultaneous method", stock solutions of 25 wt % resols in 7:3 DOX/THF were made and combined with ISV powder (2:1 ISV/resols by weight) without prior dissolution of ISV. Further DOX and THF were added thereafter (7:3 DOX/THF) to completely dissolve ISV and mix with the resols. In the "consecutive method", ISV was first dissolved in 7:3 DOX/THF. After complete dissolution, the 25 wt % resols solution was added. In both the consecutive and simultaneous methods, the ISV terpolymer and carbon precursor were dissolved at a 2:1 ratio (by weight) in a 7:3 (by weight) DOX/THF solution, while solution concentrations were varied (vide infra). It is important to note that the overall process following solution preparation for both the consecutive method and simultaneous method was kept the same - in order to ensure a direct comparison between both methods. Any differences in structural characteristics of the membranes therefore could be traced back to the differences in the preparation pathways of the casting solutions.

# Small-Angle X-ray Scattering (SAXS) of Solutions.

Figure 2 compares selected small-angle X-ray scattering (SAXS) results of the different quiescent casting solutions employing the simultaneous (Figure 2b) and consecutive (Figure 2c) solution preparation methods with those of parent ISV (no additives, Figure 2a) in order to investigate the effects of resols additives as well as the sample preparation method on order and structure as a function of solution concentration (marked for each trace). For pure ISV (Figure 2a), results for solutions ranging from 0.5 to 17 wt % ISV in 7:3 DOX/THF are exhibited. At the lowest concentration, no particular structure is evident, and a correlation peak first emerging at 4.1 wt % suggests the onset of micelle formation without ordered packing. Beyond 10 wt %, a clear lattice is evidenced by welldefined higher-order peaks consistent with a body-centered cubic (BCC) lattice with a lattice parameter of 57 nm at 17 wt %, consistent with previously reported results.<sup>40</sup>

The SAXS patterns of ISV + resols solutions prepared via the simultaneous method (Figure 2b) and ranging in concentration from 0.8 to 17 wt % (ISV + resols at 2:1 ISV/ resols weight ratio) show a similar evolution but with two major differences: First, peaks are shifted to smaller q values, suggesting larger characteristic structures consistent with resols swelling the system. Second, no specific lattice could be associated with the relatively broad first- and higher-order reflexes, even at the highest concentrations studied (see also Figure S1). Interestingly, both of these effects are reverted when the consecutive method is used for sample preparation (Figure 2c). At 17 wt %, SAXS data again suggest a BCC lattice with a lattice parameter of 63 nm, i.e., only slightly larger than the pure ISV system at the same overall concentration. Figure 2d provides the scattering pattern of a 19 wt % ISV + resols solution prepared by this method exhibiting clear resolution up to the 13th-order peak and overall peak spacing consistent with a BCC lattice with a spacing of 64 nm. To the best of our knowledge, this is the largest number of higher-order reflexes observed for an ISV-based micellar lattice in 7:3 DOX/ THF. 21,40 The individual BCC lattice reflexes sit on top of oscillations that presumably are due to the form factor of the micelles.

We hypothesize that in the simultaneous case, the addition of resols prior to dissolution of the ISV hinders the ISV polymer from forming homogeneously sized micelles and

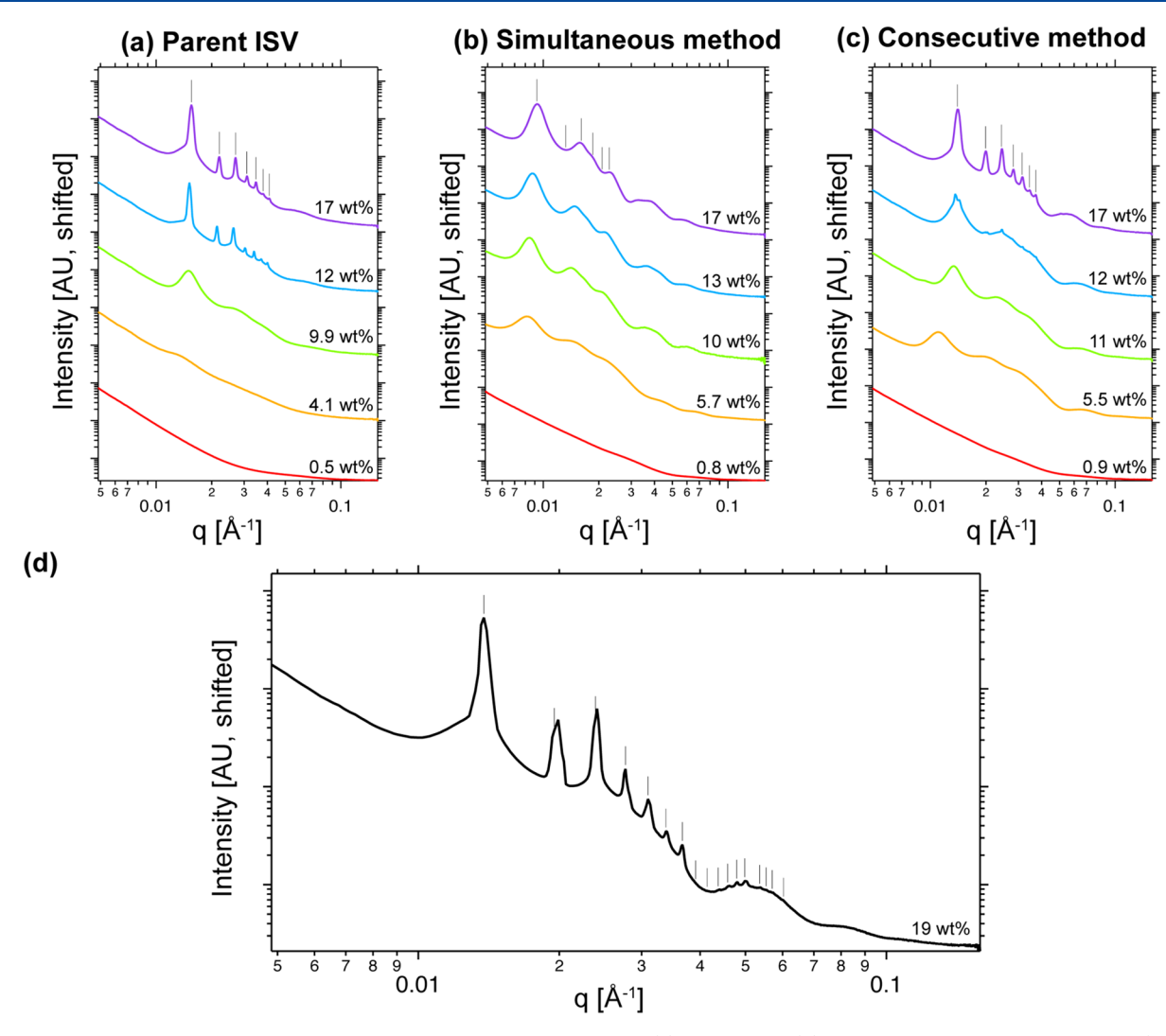


Figure 2. Small-angle X-ray scattering patterns of different polymer solutions: (a) parent ISV, (b) simultaneous method ISV + resols (2:1 ISV/resols by weight), (c) consecutive method ISV + resols (2:1 ISV/resols by weight), and (d) selected pattern of consecutive method derived solution at 19 wt % ISV + resols (2:1 ISV/resols by weight). All solutions were 7:3 DOX/THF (by weight). Tick marks indicate expected peak positions for a BCC lattice relative to the observed primary peak. The (a) ISV concentrations and (b-d) ISV + resols concentrations are reported with each trace.

therefore from forming well-ordered micellar BCC lattices in solution. In the meantime, we know from a set of independent nuclear magnetic resonance (NMR) spectroscopy studies that the P4VP block rather than the PI block of ISV in 7:3 DOX/THF forms the micelle core. <sup>41</sup> The reason why the presence of resols hinders highly ordered micelle lattice formation might be that they hydrogen-bond to the P4VP blocks upon dissolution early on, thereby locking the system into large structures that cannot equilibrate into well-defined micellar lattices. In contrast, in the consecutive case, ISV polymer micelles are allowed to form first, before addition of the resols, therefore allowing for cubic micelle lattice formation with only slightly larger lattice spacings as for the parent ISV terpolymer, presumably due to swelling of the P4VP micelle cores.

Figure S1 shows the SAXS patterns of the full concentration series studied (including points between those in Figure 2) as well as a table of concentrations versus lattice spacings based on the first-order peak position and assuming a BCC lattice in all cases. The onset of cubic ordering in the parent ISV case (Figure S1a) occurs at comparable overall concentration ( $\approx$ 12 wt %) as in the ISV + resols consecutive case (Figure S1c).

This means that in the ISV + resols case, ordering occurs at a lower ISV concentration, so a less amount of polymer is needed to obtain cubic order in solution with a similar lattice parameter. This is again consistent with swelling of the micelle cores with resols, which after mixing into the existing BCP micelle solutions may simply diffuse into the existing P4VP cores and expand their size.

In Situ Grazing-Incidence Small-Angle X-ray Scattering (GISAXS). To elucidate the behavior of this pathway-dependent system during evaporation, in situ grazing-incidence small-angle X-ray scattering (GISAXS) during blade-coating and evaporation was performed.<sup>34</sup> Details are provided in the Experimental Section. In short, films were cast with a doctor blade, and the subsequent evaporation process was monitored in situ at various times using GISAXS. During successful S/CNIPS-based membrane formation, this evaporation process can lead to long-range BCP micelle ordering as evidenced by Bragg reflection spots in the GISAXS patterns in a layer formed atop a disordered substructure.

Figure 3a—c shows the representative time-dependent *in situ* GISAXS pattern sequences for all three scenarios tested, *i.e.*, for

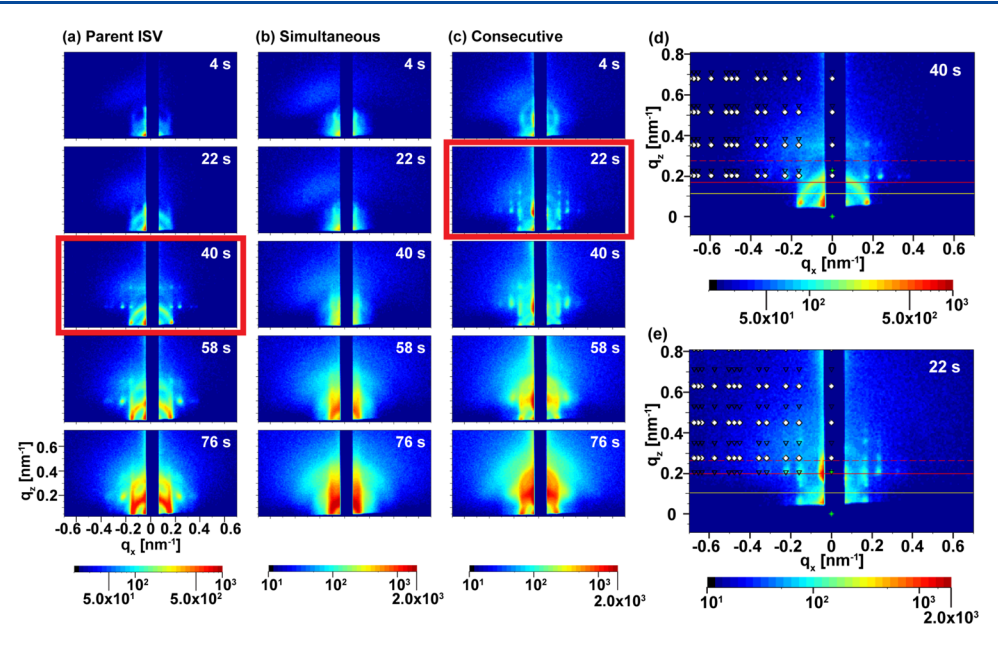


Figure 3. Selected *in situ* GISAXS patterns of solutions of (a) 10 wt % ISV, (b) 10 wt % ISV + resols simultaneous method (2:1 ISV/resols by weight), and (c) 10 wt % ISV + resols consecutive method (2:1 ISV/resols by weight) cast and evaporated for various times as indicated. The two images boxed in red at (a) 40 and (c) 22 s were indexed in panels (d) and (e), respectively. All solutions were 7:3 DOX/THF (by weight). Spot markings on the left sides in panels (d) and (e) correspond to those expected for an SC lattice with the (001) plane parallel to the surface and lattice parameters of 38 and 39.5 nm, respectively.

Table 1. Summary of *In Situ* GISAXS Pacions Indicating Suggested BCP Film Surface Lattices and Corresponding Lattice Spacings

polymer system	corresponding GISAXS pattern	system wt %	evaporation time $(s)$	observed ordered structure	lattice spacing (nm)	experimental $q^*$ $(nm^{-1})$
ISV	S2c	7.9	61	SC	39.5	0.159
ISV	3(a,d), S2d	10	40	SC	38.0	0.165
ISV + resols (simultaneous)	3b, S3	8.0, 10, 12, 15	n/a	-	_	_
ISV + resols (consecutive)	S4a, S5a	8.0	31	SC	40.5	0.155
ISV + resols (consecutive)	3(c,e), S4b, S5b	10	22	SC	39.5	0.159
ISV + resols (consecutive)	S4c, S5c	13	13	SC	39.5	0.159
ISV + resols (consecutive)	S4d, S5d	15	21	BCC	58.0	0.153

parent ISV terpolymer (a) and for ISV + resols (2:1 ISV/resols weight ratio) systems prepared either with the simultaneous (b) or consecutive (c) methods. Figures S2-S5 summarize all data sets collected together with specific indexed patterns. Figure 3a shows the in situ GISAXS patterns of a film cast from a 10 wt % solution of parent ISV terpolymer and collected at different solvent evaporation times ranging from 4 to 76 s. The film started out disordered, with very faint scattering rings evident at the earliest time point (4 s evaporation time). These scattering rings become more prominent at 22 s. The half-ring (lower ring) at smaller q is caused by transmission scattering, while the upper full ring is associated with reflection scattering. Discrete Bragg reflection spots first emerge at an evaporation time of 40 s. This marks the transition from a disordered to a highly ordered state with long-range order. As time progresses, the Bragg spots become more intense, but those on the time scale shown up to about 80 s never disappear.

In contrast, the time-dependent *in situ* GISAXS patterns over the same time interval resulting from the evaporation of a film cast from a 10 wt % ISV + resols solution (2:1 ISV/resols

weight ratio) prepared *via* the simultaneous route do not exhibit well-defined reflection spots, suggesting disordered micelle packing at all times studied (Figure 3b). Finally, the time-dependent progression of *in situ* GISAXS patterns resulting from a film that was cast from a 10 wt % ISV + resols solution (2:1 ISV/resols weight ratio) prepared *via* the consecutive method shown in Figure 3c is again more similar to that of the parent ISV polymer, except that well-defined reflections signaling long-range order appear earlier, here around 22 s rather than 40 s, and became washed out at the longest time points at the longest time points shown around 80 s.

In situ GISAXS patterns at 40 s for series (a) and 22 s for series (c) were simulated using indexGIXS. The indexed patterns are shown in Figure 3d,e, respectively. The circles and triangles indicate expected peak positions for simple cubic (SC) lattices for the directly scattered and reflected beams, respectively. The sample horizon is indicated by the yellow line, while the polymer critical angle and substrate critical angle are indicated by the solid and dashed red lines, respectively.

Table 2. Summary of Experiments Conducted to Elucidate Optimized Experimental Conditions for Obtaining Ordered Top Surfaces in Membranes Cast via the S/CNIPS Process<sup>a</sup>

polymer system	corresponding SEM figures and conditions	relative humidity (%)	substrate $T$	nonsolvent bath T	observed surface order
ISV	4a (9.9 wt %, 45 s), S6 (9.9 wt %, 30-45 s)	<30	RT	RT	cubic
ISV	S10a (10 wt %, 30-60 s)	≈70	RT	RT	_
ISV	S10b (10 wt %, 20-40 s)	≈70	30 °C	RT	cubic
ISV + resols (consecutive)	S7a (10 wt %, 30–105 s), S7b (15 wt %, 15–30 s)	<30	RT	RT	_*
ISV + resols (consecutive)	4c (10 wt %, 45 s), 5b (10 wt %, 20–40 s), S8a (10 wt %, 15–45 s), S8b (15 wt %, 10–15 s), S11 (10 wt %, 40 s), S15 (15 wt %, 5–10 s)	<30	30 °C	RT	cubic
ISV + resols (consecutive)	S11 (10 wt %, 40 s)	<30	30 °C	4 °C	cubic
ISV + resols (consecutive)	S11 (10 wt %, 40 s)	<30	30 °C	40 °C	cubic
ISV + resols (simultaneous)	S9a (10 wt %, 15–30 s)	<30	RT	RT	_
ISV + resols (simultaneous)	4b (10 wt %, 40 s), 5a (11 wt %, 20–40 s), S9b (10 wt %, 15–30 s)	<30	30 °C	RT	_

<sup>&</sup>lt;sup>a</sup>The asterisk means that the top surface order closest to cubic order was observed at the 90 s evaporation time point.

The region between the polymer and substrate critical angles is called the Yoneda band.<sup>42</sup> The patterns in Figure 3d,e for 10 wt % solutions of pure ISV at 40 s and ISV + resols prepared *via* the simultaneous method at 22 s were both indexed to an SC lattice with the (001) plane in the in-plane direction relative to the film surface and lattice parameters of 38 and 39.5 nm, respectively.

Table 1 summarizes all the quantitative in situ GISAXS analysis results with additional data sets and indexing results at varying dope concentrations provided in Figures S2-S5. In the pure ISV case, SC lattices with lattice parameters of 39.5 and 38 nm emerged for the 7.9 (Figure S2a) and 10 wt % ISV solutions (Figure 3a and Figure S2b) in 7:3 DOX/THF, respectively. For ISV + resols solutions prepared via the simultaneous method, no pattern could be ascribed to any particular lattice with long-range order (Figure 3b and Figure S3). Instead, polycrystalline structures dominated the behavior as evidenced by the formation of scattering rings (Figure S3c,d). For the consecutive case, however, all tested concentrations resulted in patterns that could be indexed to a particular lattice with long-range order (Figure S4). At lower concentrations of 8.0, 10, and 13 wt % (Figure S4a-c), the GISAXS patterns at 31, 22, and 13 s evaporation times were consistent with SC lattices with the (001) plane parallel to the surface and lattice parameters of 40.5, 39.5, and 39.5 nm, respectively, while at the highest concentration tested of 15 wt % (Figure S4d), the GISAXS pattern at the 21 s time-point was consistent with a BCC lattice with the (110) plane parallel to the film surface and a lattice parameter of 58 nm (Figure S5). This latter high concentration case was the sole example of BCC ordering in the membrane top surface layer consistent with ordering that was found for quiescent solutions at higher concentrations (Figure 2c).

These *in situ* GISAXS results obtained for our 95 kg mol<sup>-1</sup> ISV-terpolymer-based studies are consistent with those reported by Gu *et al.* for pure ISV cast films with varying molar masses and similar terpolymer composition.<sup>34</sup> They corroborate the overall picture that order in the top surface layer of these membranes evolves from disorder to BCC and then to SC lattices,<sup>41</sup> the former being consistent with solution structures at higher concentrations as observed with SAXS studies (see Figure 2) and the latter being consistent with the

pore structure of the final ISV membranes (vide infra).<sup>34</sup> The quiescent solution SAXS data in Figure 2 was obtained by keeping the DOX/THF solvent ratio constant. It should be noted that because of the different rates of evaporation of DOX and THF during SNIPS, this condition is not met during membrane formation. For a 91 kg mol<sup>-1</sup> ISV terpolymer, Gu et al. observed an SC lattice at a lower ISV concentration of 10 wt %, while solution SAXS at a higher concentration of 16 wt % confirmed a BCC lattice.<sup>34</sup> Furthermore, for a smaller, 43 kg mol<sup>-1</sup> ISV terpolymer at 16 wt %, they observed a transition from a BCC to an SC lattice, with both lattices having the same lattice orientation relative to the substrate as found in the current study. This transition has recently been ascribed to a concentration-dependent segregation of PS and PI in the micelle corona. 41 Consistent with the interpretation of results in these earlier investigations, we infer that the highest ISV + resols concentration of 15 wt % studied here for the consecutive method generates samples of sufficiently high viscosity to prevent the final BCC to SC transition, thereby trapping the system in the BCC order state.

From these results on the early membrane formation stages upon solvent evaporation after blading, the addition of resols to ISV does not seem to substantially perturb the structure formation process if, and only if, the resols are added to the terpolymer using the consecutive method. In contrast, as is revealed by these *in situ* GISAXS studies, adding ISV and resols simultaneously to the 7:3 DOX/THF solvent mixture does prevent highly ordered lattice formation.

In summary, qualitative comparison of *in situ* GISAXS with transmission solution SAXS results (*i.e.*, compare Figure 2a—c with Figure 3a—c) suggests that while parent ISV and consecutive-method-derived ISV + resols solutions and films exhibit highly ordered (cubic) lattices, those from the simultaneous method do not. For a more quantitative analysis, in particular for the consecutive method of interest here, the GISAXS pattern obtained from the 15 wt % ISV + resols solution after 21 s of evaporation (Figure S5d) and indexed to a BCC lattice with a lattice parameter of 58 nm can be directly compared to the corresponding solution SAXS results for concentrations above 15 wt %. Patterns for all these solutions could also be indexed to BCC lattices (see Figure S1c), consistent with GISAXS results, where 15 wt % only indicates

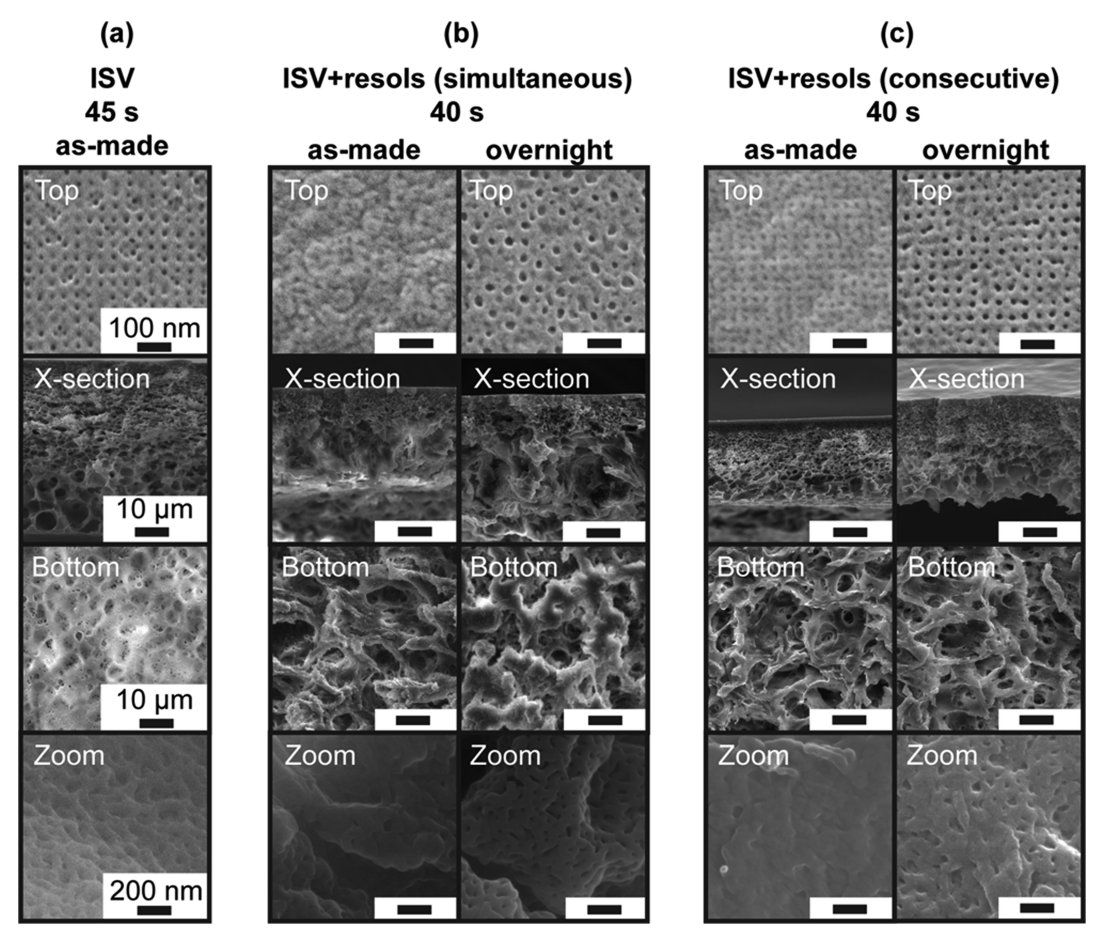


Figure 4. SEM characterization of as-made membranes prepared from (a) 9.9 wt % ISV, (b) 10 wt % ISV + resols (2:1 ISV/resols weight ratio) and via the simultaneous method, and (c) 10 wt % ISV + resols (2:1 ISV/resols weight ratio) and via the consecutive method. The solutions were in 7:3 DOX/THF, cast, and evaporated for (a) 45 s on a RT ( $\approx$ 20 °C) substrate or (b,c) 40 s on a 30 °C substrate. All films were cast at low relative humidity (<30%) and plunged into a RT ( $\approx$ 20 °C) nonsolvent DI water bath. Micrographs from top to bottom, respectively, show the top surface, cross section, bottom surface, and a zoomed-in image from the macroporous bottom region of the membrane. Scale bars are the same in all rows as indicated in images in the left-most column.

the starting solution concentration. For example, comparison to the BCC lattice parameter of 63 nm of an 18 wt % ISV + resols solution (see the table in Figure S1d) shows that the lattice parameters deviate by less than 10%. This corroborates earlier studies of ISV solutions and resulting SNIPS-derived ISV-based UF membranes, demonstrating that solution SAXS is a good predictor of the UF membrane surface structure. The consecutive studies, this conclusion also seems to hold for consecutive-method-derived ISV + resols mixed membranes.

Characterization of As-Made Membranes via Scanning Electron Microscopy (SEM). Following X-ray solution and *in situ* evaporation studies, membranes cast *via* the CNIPS process were characterized in the as-made state using scanning electron microscopy (SEM).

As-made is defined as being the state immediately following precipitation in the nonsolvent bath before any thermal treatment. Alternatively, after casting, some membranes were left in the DI water bath overnight under stirring in order to provide enough time for the resols to be washed out. We expected that this processing would improve visualization of porosity *via* SEM.

In order to screen for optimal membrane structure formation, various parameters including evaporation time, substrate temperature, and water bath conditions were tested. A summary of the results from varied substrate temperatures as well as nonsolvent bath temperatures is provided in Table 2, while the full set of scanning electron micrographs is provided in Figures S6–S11. While casting at room temperature resulted in ordered top surfaces for the pure ISV dopes (Figure S6), such conditions did not result in optimal surface ordering from ISV + resols dopes (see results for the consecutive method in Figure S7, where the closest to cubic order was observed at the 90 s evaporation time point). To search for experimental conditions for improved top surface ordering, the casting substrate temperature was varied. Instead of a room-temperature substrate, membranes were cast on a 30 °C substrate. This resulted in substantially improved top surface order for both 10 and 15 wt % ISV + resols casting solutions using the consecutive method (compare results in Figure S8 with those in Figure S7). When the heated substrate approach was applied to the simultaneous preparation method, it failed to improve the top surface order (Figure S9). When it was applied together with increased humidity casting conditions (≈70% relative humidity) for the pure parent ISV system, which resulted in poor ordering on room-temperature substrates under these conditions, it indeed helped improve the order of the top surface of the material (Figure S10). Finally, for the consecutive method, three water bath temperatures were tested to probe their effects on membrane top surface order (Figure

# (a) As-made (simultaneous method) (b) As-made (consecutive method) 20 s 40 s 20 s 30 s 30 s50 nm 50 nm 30 s 40 s 20 s 30 s 10 µm 10 µm (c) Carbonized (simultaneous method) (d) Carbonized (consecutive method) 30 9 40 s 30 < 50 nm 50 nm 40 s 20 s 40 s 20 s 30 s

Figure 5. Top surface (top rows) and cross-sectional (bottom rows) SEM characterization of (a) as-made and (c) corresponding carbonized membranes prepared via the simultaneous method from an 11 wt % ISV + resols (2:1 ISV/resols weight ratio) solution in 7:3 DOX/THF. SEM characterization of (b) as-made and (d) corresponding carbonized membranes prepared via the consecutive method from a 10 wt % ISV + resols (2:1 ISV/resols weight ratio) solution in 7:3 DOX/THF. The films were cast at the same height. However, with increased evaporation time from 20 to 40 s (left to right), more solvent evaporates, producing denser and thus thinner thickness membranes. The films were cast at low relative humidity (<30%) onto a 30 °C-heated substrate and allowed to evaporate for various amounts of time (20–40 s, as indicated) before being plunged into a RT ( $\approx$ 20 °C) nonsolvent DI water bath. The scale is the same for all rows as indicated by scale bars on the left side.

5 µm

S11). When dipping into DI water baths at room temperature ( $\approx$ 20 °C, left images) and 4 °C (right images), the cubic order that developed during the evaporation was preserved, whereas when dipping into a warmed 40 °C (middle images) bath, the order was not preserved. Figure 4 shows SEM characterization results for optimized membrane formation conditions, i.e., cast at low relative humidity (<30%), evaporated for 45 s on RT  $(\approx 20 \, ^{\circ}\text{C}, (a))$  or 40 s on 30  $^{\circ}\text{C}$  (b,c) substrates, before being plunged into a RT (≈20 °C) nonsolvent DI water bath, obtained from the following polymer dope solutions in 7:3 DOX/THF: 9.9 wt % parent ISV (Figure 4a), 10 wt % ISV + resols (2:1 ISV/resols weight ratio) simultaneous method (Figure 4b), and 10 wt % ISV + resols (2:1 ISV/resols weight ratio) consecutive method (Figure 4c). For both simultaneous and consecutive cases, membrane samples were taken following 30 s of exposure to the nonsolvent DI water bath (left column) and overnight stirring (right column) in the nonsolvent DI water bath (vide supra). As is evident from these images, good quality surface ordering was achieved for both the parent ISV membrane and for the membrane obtained from the consecutive method. In contrast, well-ordered top surface layers of membranes formed using the simultaneous method were not observed, consistent with X-ray scattering results reported in the previous sections. Fast Fourier transform (FFT) analysis of top surface order (Figure S12), while not applicable to membranes obtained from the simultaneous method (Figure S12b), yielded pore-to-pore distances (based on the  $q^*$  position and assuming square

5 µm

lattices) of 39 nm for the parent ISV case (Figure S12a) and 32 (red, as-made) and 40 nm (blue, overnight stirring) for consecutive-method-derived membranes (Figure S12c). These results were consistent with those obtained by manually measuring >50 pore-to-pore (channel-to-channel) distances using the measuring tool in ImageJ (data not shown). These results can be compared with the corresponding *in situ* GISAXS-derived values of 38 and 39.5 nm for 10 wt % ISV-and ISV + resols-derived membranes, respectively (see Table 1).

Heat-Treatment of As-Made Membranes and Comparison to Carbonized Materials. Once optimized parameters (low, <30% relative humidity, 30 °C-heated substrate, RT,  $\approx$ 20 °C nonsolvent DI water bath) leading to ordered top surfaces in the organic—organic (ISV-resols) hybrid membranes were identified, these membranes were subjected to a series of heat-treatments to produce CGM-C materials. Immediately following casting and precipitation, asmade membranes were dried at room temperature and then underwent heat-treatment at 130 °C, both in a vacuum oven, in order to cross-link the resols. After heat-treatment to this moderate temperature (*i.e.*, below polymer decomposition temperatures), surface features became less prominent and pores appeared to close (Figure S13).

After cross-linking, the membranes were heat-treated in a flow furnace under an inert atmosphere (nitrogen) at 1  $^{\circ}$ C min $^{-1}$  to 600  $^{\circ}$ C and held there for 3 h followed by ramping to 900  $^{\circ}$ C at 5  $^{\circ}$ C min $^{-1}$  and holding there for 3 h. In this

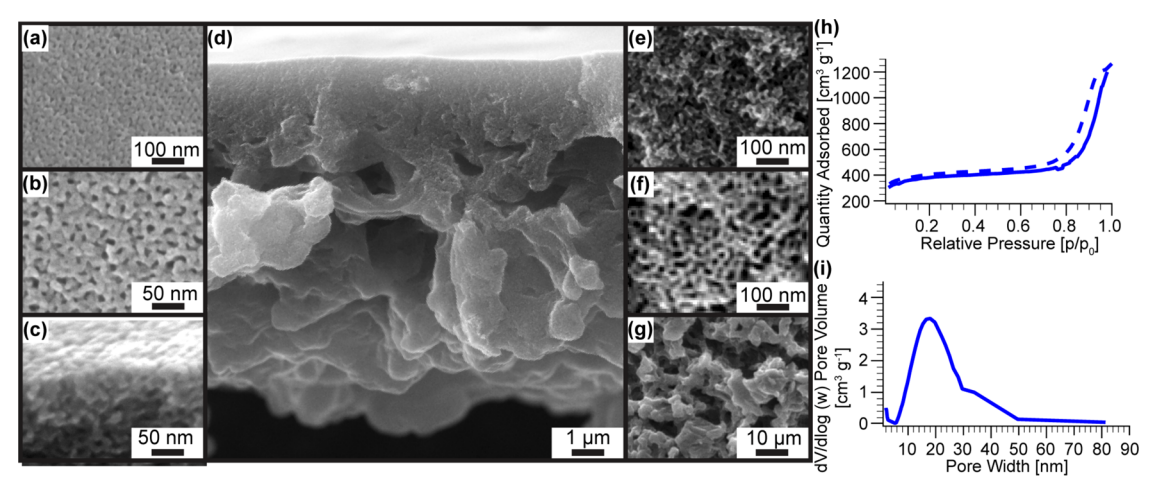


Figure 6. Characterization of CGM-C materials derived from membranes that were obtained from 11 wt % ISV + resols (2:1 ISV/resols weight ratio) solutions in 7:3 DOX/THF prepared via the simultaneous method, cast onto a 30 °C-heated substrate, allowed to evaporate in low relative humidity conditions (<30%) for 40 s before being plunged into a RT ( $\approx$ 20 °C) nonsolvent DI water bath, dried, cross-linked at 130 °C for <24 h, and carbonized. The temperature profile for the carbonizing step was first heating at a rate of 1 °C min<sup>-1</sup> to 600 °C. The temperature was held at 600 °C for 3 h before being further ramped at 5 °C min<sup>-1</sup> to 900 °C, where it was held for another 3 h before being allowed to cool back to room temperature. (a–g) Scanning electron micrographs: (a–c) top surface images at different magnifications and angles, (d) full asymmetric cross section, (e) mesoporous middle part of the cross section, (f) higher-magnification mesoporous middle part of the cross section, and (g) macroporous bottom. (h) Nitrogen sorption isotherms of the carbonized material. (i) BJH-derived pore size distribution of the final carbonized membrane material.

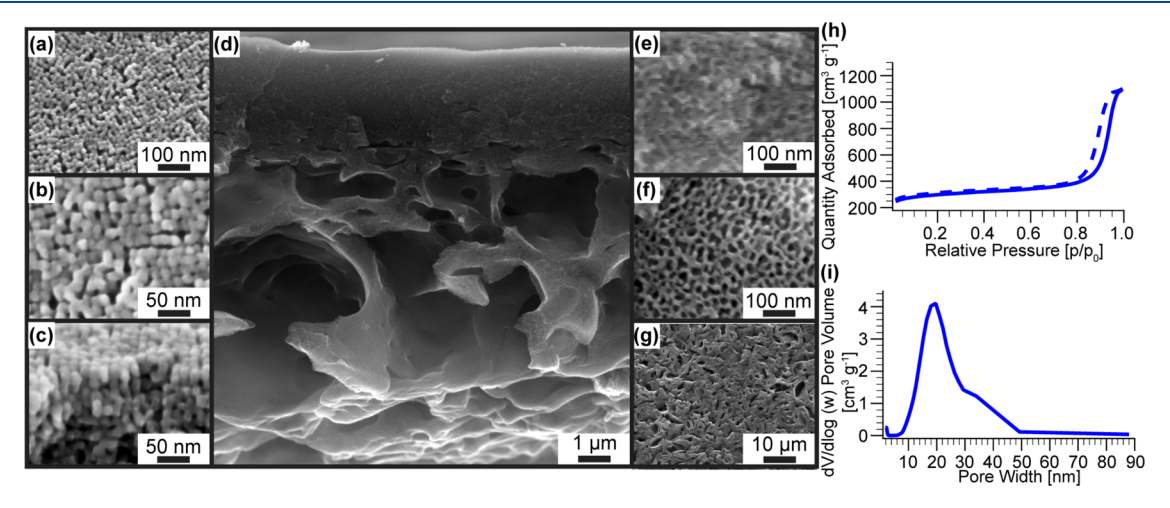


Figure 7. Characterization of the CGM-C material derived from membranes that were obtained from 10 wt % ISV + resols (2:1 ISV/resols weight ratio) solutions in 7:3 DOX/THF prepared via the consecutive method, cast onto a 30 °C-heated substrate, allowed to evaporate in low relative humidity conditions (<30%) for 40 s before being plunged into a RT ( $\approx$ 20 °C) nonsolvent DI water bath, dried, cross-linked at 130 °C for <24 h, and carbonized. The temperature profile for the carbonizing step was first heating at a rate of 1 °C min<sup>-1</sup> to 600 °C. The temperature was held at 600 °C for 3 h before being further ramped at 5 °C min<sup>-1</sup> to 900 °C, where it was held for another 3 h before being allowed to cool back to room temperature. (a–g) Scanning electron micrographs: (a–c) top surface at different magnifications and angles, (d) full asymmetric cross section, (e) mesoporous middle part of the cross section, and (g) macroporous bottom. (h) Nitrogen sorption isotherms of the carbonized material. (i) BJH-derived pore size distribution of the final carbonized material.

process, the polymer decomposed (Figure S14). However, the structure was preserved due to the cross-linked resols, which were converted into a carbon material as described and analyzed in depth in previous publications. Figure 5 provides a comparison by means of SEM characterization of membrane top surfaces (top rows) and cross sections (bottom rows) between as-made membranes prepared from 11 and 10 wt % ISV + resols (2:1 ISV/resols weight ratio) solutions in 7:3 DOX/THF *via* simultaneous and consecutive methods, respectively, and their carbonized counterparts.

In the simultaneous method as-made case (Figure 5a), a disordered mesoporous top surface transitioned into a support

structure of about 20  $\mu$ m thickness with asymmetric porosity. Figure 5a also shows that while overall features remained similar, increasing the evaporation time resulted in a denser and thinner cross section, likely due to the evaporation of more solvent out of the membrane. Thus, the evaporation time provides a pathway to tuning the porosity profile and thus surface accessibility of and transport through the asymmetric structure. When this organic—organic hybrid material was carbonized (Figure 5c), the overall asymmetric structure was retained. However, due to material loss and associated material shrinkage, membrane thickness was reduced to about 10  $\mu$ m (compare cross-sectional scale bars in Figure 5a,c). Finally, this

SEM analysis demonstrates that an increased evaporation time resulted in smaller feature sizes on the mesoporous top surface.

For the consecutive method as-made and carbonized cases (Figure 5b,d), general trends were the same as described for the simultaneous method. The main difference, however, was the highly ordered, cubic top surface order of the as-made materials, in particular at longer evaporation times, which was retained in the final carbonized membranes. Similar results were obtained for membranes that were cast from a 15 wt % ISV + resols solution (Figure S15).

**Characterization of Carbon Materials.** A more in-depth characterization of CGM-C materials prepared *via* both the simultaneous and consecutive methods using SEM and nitrogen sorption analysis is shown in Figures 6 and 7, respectively.

The carbon materials resulting from the simultaneous method possessed a homogeneous top surface but with only disordered arrays of mesopores (Figure 6a,b). In contrast, for carbon materials obtained from the consecutive method employing optimized membrane formation parameters, a top surface with periodic local cubic order was achieved (Figure 7a,b). It is evident from comparing these SEM images with those of the parent ISV membrane or the ISV + resols consecutive-method-derived as-made/overnight samples (e.g., see Figure 4a,c) that the original array of square ordered mesopores in the top surface layer of these materials is replaced by square ordered arrays of dimples in the carbonized materials. We therefore conclude that in the top surface layer, the resulting carbon material stems from resols that originally filled the P4VP-coated (pore) space of the ISV membrane in the co-assembly process. This square ordering extends a few micelle layers down along the film normal (Figure 7c) before the order is lost in the meso- to macroporous substructure.

Simultaneous and consecutive methods resulted in porous asymmetric carbon structures (Figures 6d and 7d) with mesoporosity throughout the material. This porosity was characterized via nitrogen sorption isotherms analyzed using the Brunauer-Emmett-Teller (BET) method (Figures 6h and 7h). Type-IV curves with H1-type hysteresis and sharp capillary condensations above relative pressures of 0.9 were observed in both cases. For the simultaneous method, a BET surface area of 1322 m<sup>2</sup> g<sup>-1</sup> with a weighing error of 357 m<sup>2</sup> g<sup>-1</sup>, micropore area of 837 m<sup>2</sup> g<sup>-1</sup>, and specific pore volume of 1.96 cm<sup>3</sup> g<sup>-1</sup> at  $p/p_0 = 0.99$  were obtained. For the consecutive method, a slightly lower BET surface area of 1024 m<sup>2</sup> g<sup>-1</sup> with a weighing error of 143 m $^2$  g $^{-1}$ , micropore area of 655 m $^2$  g $^{-1}$ , and specific pore volume of 1.69 cm<sup>2</sup> g<sup>-1</sup> at  $p/p_0 = 0.99$  were obtained. Barrett-Joyner-Halenda (BJH) pore size distributions of materials prepared from both methods had similar profiles (Figures 6i and 7i). For the material from the simultaneous method, the pore size distribution peaked at 18 nm with a fwhm of 15 nm, while for the material from the consecutive method, the values were 20 and 12 nm for peak pore size and fwhm, respectively. Although the volumetric surface area was not determined here, in a separate study on the use of these carbon membranes in EDLCs, 28 a volumetric surface area of 36 m<sup>2</sup> cm<sup>-3</sup> was reported for the asymmetric carbons prepared via the consecutive method.

# CONCLUSIONS

We reported a successful non-equilibrium-type one-pot synthesis method to obtain porous carbon materials with a structurally asymmetric pore profile and well-defined mesoporosity throughout the material (CMG-Cs). These materials possess ordered top-surface layers and hierarchical substructures with meso- to macropores. To that end, approaches were pursued in which carbon precursors (resols) were either simultaneously or consecutively mixed with the structure directing triblock terpolymer, ISV. Both methods generally resulted in approximately 10 micron-thick carbon materials with a mesoporous top surface layer, which continued into a structurally asymmetric support structure with increasing pore size along the film normal, ending in an open and macroporous structure at the membrane bottom. The walls of the macroporous support are also mesoporous providing an additional structural hierarchy. The difference between the two methods is that only after carefully screening various processing conditions, the optimized consecutive method resulted in a periodically ordered top surface layer in the resulting porous carbon materials. In the consecutive method, ISV was first dissolved in a 7:3 DOX/THF solvent mixture, before the addition of resols, which likely allows for the formation of uniform micelles in solution prior to the addition of hydrogen bonding additive and therefore allows for the evolution of highly ordered solution structures with increasing concentration as evidenced by SAXS of quiescent ISV + resols solutions. Upon solvent evaporation, this order also occurs in the top surface layer of as-made asymmetric membranes as evidenced by in situ GISAXS experiments and SEM images of the resulting top surfaces of the final carbon materials. In contrast to the consecutive method, even after carefully screening a variety of processing conditions, the simultaneous method (in which resols are already present when the polymer dissolves and forms micelles) only resulted in relatively disordered structures both in quiescent solutions and in the resulting membranes as evidenced by SAXS, in situ GISAXS, and SEM of the final carbons.

We expect that the insights gained by these fundamental solution and evaporation studies will aid in expanding the types of additives, which can be combined with polymers in the CNIPS process, while successfully maintaining the characteristic well-ordered top surfaces of SNIPS membranes. This periodic order of the pores in the top separation layer, together with the tunable asymmetric and simultaneously hierarchical porosity of the substructure with mesopores throughout the material, is expected to combine high surface area with high flux (e.g., periodically ordered pores generate a higher pore density, in turn increasing flux). We have recently demonstrated the beneficial effects of this membrane architecture on the creation of EDLCs with record-setting performance.<sup>2</sup> However, due to the advantages of high porosity and pore accessibility as well as the proven scalability of the C/SNIPSbased membrane formation process, we also expect these asymmetric carbon materials to find use in other areas of energy conversion and storage as well as in catalysis and separations.

# ASSOCIATED CONTENT

# Supporting Information

The Supporting Information is available free of charge at https://pubs.acs.org/doi/10.1021/acs.macromol.0c02720.

Additional SAXS of solutions, GISAXS of films, and additional characterization in the form of scanning electron micrographs of as-made and heat-treated membranes (PDF)

# AUTHOR INFORMATION

## Corresponding Author

Ulrich Wiesner — Department of Materials Science and Engineering, Cornell University, Ithaca, New York 14853, United States; ● orcid.org/0000-0001-6934-3755; Email: ubw1@cornell.edu

#### **Authors**

Sarah A. Hesse — Department of Materials Science and Engineering, Cornell University, Ithaca, New York 14853, United States; Department of Chemistry and Chemical Biology, Cornell University, Ithaca, New York 14853, United States; Occid.org/0000-0002-2383-4476

Peter A. Beaucage — Department of Materials Science and Engineering, Cornell University, Ithaca, New York 14853, United States; Occid.org/0000-0002-2147-0728

Detlef-M. Smilgies — Cornell High Energy Synchrotron Source (CHESS), Wilson Laboratory and R. F. Smith School of Chemical and Biomolecular Engineering, Cornell University, Ithaca, New York 14853, United States; orcid.org/0000-0001-9351-581X

Complete contact information is available at: https://pubs.acs.org/10.1021/acs.macromol.0c02720

#### **Author Contributions**

S.A.H. and U.W. came up with the idea. S.A.H. performed the experiments. P.A.B. set up and helped perform and analyze the X-ray experiments, while D.-M.S. developed and set up the *in situ* doctor blading apparatus at the beamline D1 at CHESS and helped in analysis and interpretation of the experimental GISAXS results. S.A.H. and U.W. wrote the manuscript, with all authors reading and providing feedback on the manuscript.

#### Notes

The authors declare the following competing financial interest(s): S.A.H., P.A.B., and U.W. declare that they have submitted a patent disclosure based in part on this study through Cornell University. U.W. declares a competing financial interest in the start-up Terapore Technologies, Inc.

# ACKNOWLEDGMENTS

This work was funded by the National Science Foundation under award DMR-1707836. This work is based upon research conducted at the Cornell High Energy Synchrotron Source (CHESS), which is supported by the National Science Foundation under award DMR-1332208. This work made further use of the Cornell Center for Materials Research Shared Facilities, which are supported through the NSF MRSEC program (DMR-1719875). P.A.B. was supported by the National Science Foundation Graduate Research Fellowship Program (DGE-1650441). S.A.H. acknowledges Wiesner Group (Cornell University) members Y. Hibi, R. P. Thedford, and K. P. Barteau for help in casting membranes at the CHESS D1 beamline, Q. Zhang for help in indexing pure ISV GISAXS patterns, and J. G. Werner for helpful discussions.

# ABBREVIATIONS

EDLC, electrochemical double-layer capacitor; SA, self-assembly; BCP, block copolymer; NIPS, non-solvent-induced phase separation; PAN, polyacrylonitrile; SNIPS, self-assembly and nonsolvent-induced phase separation; SV, poly(isoprene)-b-poly(2-vinylpyridine); UF, ultrafiltration; CNIPS, co-assembly and non-solvent-induced phase separation; ISV, poly-

(isoprene)-b-poly(styrene)-b-poly(4-vinylpyridine); EES, electrochemical energy storage; resols, phenol formaldehyde resols carbon precursor; TiN, titanium nitride; THF, tetrahydrofuran; DOX, 1,4-dioxane; DI, deionized; PDI, polydispersity index; <sup>1</sup>H NMR, <sup>1</sup>H solution nuclear magnetic resonance; GPC, gel permeation chromatograph; RI, refractive index; RT, room temperature; SAXS, small-angle X-ray scattering; CHESS, Cornell High Energy Synchrotron Source; BCC, body-centered cubic; GISAXS, grazing-incidence small-angle X-ray scattering; SEM, scanning electron microscopy; FFT, fast Fourier transform; TGA, thermogravimetric analyzer; BET, Brunaer–Emmett–Teller; BJH, Barrett–Joyner–Halenda; fwhm, full width at half-maximum; CGM-Cs, carbon-based Cornell Graded Materials

# REFERENCES

- (1) Rolison, D. R.; Long, J. W.; Lytle, J. C.; Fischer, A. E.; Rhodes, C. P.; McEvoy, T. M.; Bourg, M. E.; Lubers, A. M. Multifunctional 3D Nanoarchitectures for Energy Storage and Conversion. *Chem. Soc. Rev.* 2009, 38, 226–252.
- (2) Orilall, M. C.; Wiesner, U. Block Copolymer Based Composition and Morphology Control in Nanostructured Hybrid Materials for Energy Conversion and Storage: Solar Cells, Batteries, and Fuel Cells. *Chem. Soc. Rev.* **2011**, *40*, 520–535.
- (3) Werner, J. G.; Rodríguez-calero, G. G.; Abruña, H. D.; Wiesner, U. Block Copolymer Derived Multifunctional Gyroidal Monoliths for 3-D Electrical Energy Storage Applications. arXiv:1706.02134 [physics.chem-ph] 2017.
- (4) Wang, X.; Li, W.; Chen, Z.; Waje, M.; Yan, Y. Durability Investigation of Carbon Nanotube as Catalyst Support for Proton Exchange Membrane Fuel Cell. *J. Power Sources* **2006**, *158*, 154–159.
- (5) Ismail, A. F.; David, L. I. B. A Review on the Latest Development of Carbon Membranes for Gas Separation. *J. Membr. Sci.* **2001**, *193*, 1–18
- (6) Werner, J. G.; Rodríguez-Calero, G. G.; Abruña, H. D.; Wiesner, U. Block Copolymer Derived 3-D Interpenetrating Multifunctional Gyroidal Nanohybrids for Electrical Energy Storage. *Energy Environ. Sci.* **2018**, *11*, 1261–1270.
- (7) Lee, J.; Yoon, S.; Hyeon, T.; Oh, S. M.; Kim, K. B. Synthesis of a New Mesoporous Carbon and Its Application to Electrochemical Double-Layer Capacitors. *Chem. Commun.* **1999**, *0*, 2177–2178.
- (8) Ryoo, R.; Joo, S. H.; Jun, S. Synthesis of Highly Ordered Carbon Molecular Sieves via Template-Mediated Structural Transformation. *J. Phys. Chem. B* **1999**, *103*, 7743–7746.
- (9) Jun, S.; Joo, S. H.; Ryoo, R.; Kruk, M.; Jaroniec, M.; Liu, Z.; Ohsuna, T.; Terasaki, O. Synthesis of New, Nanoporous Carbon with Hexagonally Ordered Mesostructure. *J. Am. Chem. Soc.* **2000**, *122*, 10712–10713.
- (10) Liang, C.; Hong, K.; Guiochon, G. A.; Mays, J. W.; Dai, S. Synthesis of a Large-Scale Highly Ordered Porous Carbon Film by Self-Assembly of Block Copolymers. *Angew. Chem., Int. Ed.* **2004**, *43*, 5785–5789.
- (11) Tanaka, S.; Nishiyama, N.; Egashira, Y.; Ueyama, K. Synthesis of Ordered Mesoporous Carbons with Channel Structure from an Organic-Organic Nanocomposite. *Chem. Commun.* **2005**, *0*, 2125–2127.
- (12) Kosonen, H.; Valkama, S.; Nykänen, A.; Toivanen, M.; ten Brinke, G.; Ruokolainen, J.; Ikkala, O. Functional Porous Structures Based on the Pyrolysis of Cured Templates of Block Copolymer and Phenolic Resin. *Adv. Mater.* **2006**, *18*, 201–205.
- (13) Werner, J. G.; Hoheisel, T. N.; Wiesner, U. Synthesis and Characterization of Gyroidal Mesoporous Carbons and Carbon Monoliths with Tunable Ultralarge Pore Size. *ACS Nano* **2014**, *8*, 731–743.
- (14) Wang, D.-W.; Li, F.; Liu, M.; Lu, G. Q.; Cheng, H.-M. 3D Aperiodic Hierarchical Porous Graphitic Carbon Material for High-

- Rate Electrochemical Capacitive Energy Storage. Angew. Chem., Int. Ed. 2008, 47, 373-376.
- (15) Lin, T.; Chen, I.-W.; Liu, F.; Yang, C.; Bi, H.; Xu, F.; Huang, F. Nitrogen-Doped Mesoporous Carbon of Extraordinary Capacitance for Electrochemical Energy Storage. *Science* **2015**, *350*, 1508–1513.
- (16) Ulbricht, M. Advanced Functional Polymer Membranes. *Polymer* **2006**, 47, 2217–2262.
- (17) Wu, Y.; Liu, Z.; Ran, F. New Comprehensions on Structure Superiority of Asymmetric Carbon Membrane and Controlled Construction of Advanced Hierarchical Inner-Structure for High Performance Supercapacitors. *Microporous Mesoporous Mater.* 2019, 275, 14–25.
- (18) Yang, X.; Chen, Y.; Wang, M.; Zhang, H.; Li, X.; Zhang, H. Phase Inversion: A Universal Method to Create High-Performance Porous Electrodes for Nanoparticle-Based Energy Storage Devices. *Adv. Funct. Mater.* **2016**, *26*, 8427–8434.
- (19) Ran, F.; Shen, K.; Tan, Y.; Peng, B.; Chen, S.; Zhang, W.; Niu, X.; Kong, L.; Kang, L. Activated Hierarchical Porous Carbon as Electrode Membrane Accommodated with Triblock Copolymer for Supercapacitors. *J. Membr. Sci.* **2016**, *514*, 366–375.
- (20) Peinemann, K. V.; Abetz, V.; Simon, P. F. W. Asymmetric Superstructure Formed in a Block Copolymer via Phase Separation. *Nat. Mater.* **2007**, *6*, 992–996.
- (21) Dorin, R. M.; Marques, D. S.; Sai, H.; Vainio, U.; Phillip, W. A.; Peinemann, K.-V.; Nunes, S. P.; Wiesner, U. Solution Small-Angle X-Ray Scattering as a Screening and Predictive Tool in the Fabrication of Asymmetric Block Copolymer Membranes. *ACS Macro Lett.* **2012**, *1*, 614–617.
- (22) Dorin, R. M.; Sai, H.; Wiesner, U. Hierarchically Porous Materials from Block Copolymers. *Chem. Mater.* **2014**, 26, 339–347.
- (23) Phillip, W. A.; Dorin, R. M.; Werner, J.; Hoek, E. M. V.; Wiesner, U.; Elimelech, M. Tuning Structure and Properties of Graded Triblock Terpolymer-Based Mesoporous and Hybrid Films. *Nano Lett.* **2011**, *11*, 2892–2900.
- (24) Gu, Y.; Werner, J. G.; Dorin, R. M.; Robbins, S. W.; Wiesner, U. Graded Porous Inorganic Materials Derived from Self-Assembled Block Copolymer Templates. *Nanoscale* **2015**, *7*, 5826–5834.
- (25) Gu, Y.; Dorin, R. M.; Wiesner, U. Asymmetric Organic-Inorganic Hybrid Membrane Formation via Block Copolymer-Nanoparticle Co-Assembly. *Nano Lett.* **2013**, *13*, 5323–5328.
- (26) Hesse, S. A.; Werner, J. G.; Wiesner, U. One-Pot Synthesis of Hierarchically Macro- and Mesoporous Carbon Materials with Graded Porosity. ACS Macro Lett. 2015, 4, 477–482.
- (27) Pendergast, M. M.; Mika Dorin, R.; Phillip, W. A.; Wiesner, U.; Hoek, E. M. V. Understanding the Structure and Performance of Self-Assembled Triblock Terpolymer Membranes. *J. Membr. Sci.* **2013**, 444, 461–468.
- (28) Hesse, S. A.; Fritz, K. E.; Beaucage, P. A.; Thedford, R. P.; Yu, F.; DiSalvo, F. J.; Suntivich, J.; Wiesner, U. Materials Combining Asymmetric Pore Structures with Well-Defined Mesoporosity for Energy Storage and Conversion. ACS Nano 2020, 14, 16897–16906.
- (29) Meng, Y.; Gu, D.; Zhang, F.; Shi, Y.; Yang, H.; Li, Z.; Yu, C.; Tu, B.; Zhao, D. Ordered Mesoporous Polymers and Homologous Carbon Frameworks: Amphiphilic Surfactant Templating and Direct Transformation. *Angew. Chem., Int. Ed.* **2005**, *44*, 7053–7059.
- (30) Meng, Y.; Gu, D.; Zhang, F.; Shi, Y.; Cheng, L.; Feng, D.; Wu, Z.; Chen, Z.; Wan, Y.; Stein, A.; et al. A Family of Highly Ordered Mesoporous Polymer Resin and Carbon Structures from Organic-Organic Self-Assembly. *Chem. Mater.* **2006**, *18*, 4447–4464.
- (31) Ilavsky, J.; Jemian, P. R. *Irena*: Tool Suite for Modeling and Analysis of Small-Angle Scattering. *J. Appl. Crystallogr.* **2009**, 42, 347–353
- (32) Ilavsky, J. *Nika*: Software for Two-Dimensional Data Reduction. *J. Appl. Crystallogr.* **2012**, *45*, 324–328.
- (33) Smilgies, D. M.; Li, R.; Giri, G.; Chou, K. W.; Diao, Y.; Bao, Z.; Amassian, A. Look Fast: Crystallization of Conjugated Molecules during Solution Shearing Probed *in-Situ* and in Real Time by X-Ray Scattering. *Phys. Status Solidi RRL* **2013**, *7*, 177–179.

- (34) Gu, Y.; Dorin, R. M.; Tan, K. W.; Smilgies, D.-M.; Wiesner, U. *In Situ* Study of Evaporation-Induced Surface Structure Evolution in Asymmetric Triblock Terpolymer Membranes. *Macromolecules* **2016**, 49, 4195–4201.
- (35) Smilgies, D.-M.; Blasini, D. R. Indexation Scheme for Oriented Molecular Thin Films Studied with Grazing-Incidence Reciprocal-Space Mapping. *J. Appl. Crystallogr.* **2007**, *40*, 716–718.
- (36) Busch, P.; Rauscher, M.; Smilgies, D.-M.; Posselt, D.; Papadakis, C. M. Grazing-Incidence Small-Angle X-Ray Scattering from Thin Polymer Films with Lamellar Structures The Scattering Cross Section in the Distorted-Wave Born Approximation. *J. Appl. Crystallogr.* **2006**, *39*, 433–442.
- (37) Brunauer, S.; Emmett, P. H.; Teller, E. Adsorption of Gases in Multimolecular Layers. *J. Am. Chem. Soc.* **1938**, *60*, 309–319.
- (38) Sing, K. S. W.; Everett, D. H.; Haul, R. A. W.; Moscou, L.; Pierotti, R. A.; Rouquérol, J.; Siemieniewska, T. Reporting Physisorption Data for Gas/Solid Systems With Special Reference to the Determination of Surface Area and Porosity (Recommendations 1984). Pure Appl. Chem. 1985, 57, 603–619.
- (39) Barrett, E. P.; Joyner, L. G.; Halenda, P. P. The Determination of Pore Volume and Area Distributions in Porous Substances. I. Computations from Nitrogen Isotherms. *J. Am. Chem. Soc.* **1951**, *73*, 373–380.
- (40) Dorin, R. M.; Phillip, W. A.; Sai, H.; Werner, J.; Elimelech, M.; Wiesner, U. Designing Block Copolymer Architectures for Targeted Membrane Performance. *Polymer* **2014**, *55*, 347–353.
- (41) Hibi, Y.; Hesse, S. A.; Yu, F.; Yu, F.; Thedford, R. P.; Wiesner, U. Structural Evolution of Ternary Amphiphilic Block Copolymer Solvent Systems for Phase Inversion Membrane Formation. *Macromolecules* **2020**, *53*, 4889–4900.
- (42) Yoneda, Y. Anomalous Surface Reflection of X Rays. *Phys. Rev.* 1963, 131, 2010–2013.